Grid Impedance Characterization To Provide a Robust Phase-Locked Loop Design for PV Systems

Mohammad Jafarian, *Member, IEEE*, Ramy Ali, *Student Member, IEEE*, Valentin Rigoni, *Member, IEEE*, Terence O'Donnell, *Senior Member, IEEE*, Andrew Keane, *Senior Member, IEEE*
School of Electrical & Electronic Engineering
University College Dublin
Dublin, Ireland
mohammad.jafarian@ucd.ie, ramy.ali@ucdconnect.ie, valentin.rigoni1@ucd.ie, terence.odonnell@ucd.ie, andrew.keane@ucd.ie

***Abstract*—The operation of rooftop photovoltaic (PV) systems can be challenged by the electric characteristics of the low voltage (LV) feeders. On this subject, high-impedance LV feeders can result in PVs facing the loss of synchronization due to instability in the phase-locked loop (PLL) unit of their inverter, mainly because PLLs are commonly designed to operate under nominal grid conditions and their performance can be highly affected when the loading of the feeder deviates from the nominal one. One way to avoid such a problem is by characterizing the network impedance at the PV connection point, and use this characterization to provide a robust PLL design. This paper presents a methodology to construct a stochastic representation of the network impedance seen at the PV point of connection. To do so, the distribution of the grid resistance and inductance, under various operational scenarios, is extracted using a Monte Carlo simulation framework and then modeled via a Gaussian distribution. This distribution is employed to obtain an ellipse that embraces the values of the aforementioned resistance and inductance. This ellipse determines the range of the variations of the network impedance to be regarded in the robust design of the PLL.**

***Index Terms*—dynamic stability, low voltage distribution networks, maximum likelihood estimation, phase-locked loop, rooftop solar photovoltaic systems, stochastic modeling.**

I. Introduction

The growing adoption of rooftop solar photovoltaic (PV) systems in residential buildings is rapidly increasing the penetration of this technology in low voltage (LV) distribution systems. Besides the common technical problems associated with large PV penetrations in LV grids, e.g., over-voltages, and harmonics, another important challenge towards rooftop PV integration is concerned with retaining the stable operation of the voltage source inverter (VSI) interfacing the PV with the grid, under all expected network operational conditions. The main function of this unit is to capture the frequency and phase angle of the grid voltage and employing it in its control loops to construct a rotating reference frame to perform the abc to dq transformation [1]. One of the most applied PLL designs is the synchronous reference structure consisting of a PI controller and a voltage-controlled oscillator. In [2], different PLL structures are compared.

When integrating PV systems in weak LV grids, there are a series of aspects that must be considered in order to ensure the stability of VSI during operation. Firstly, it is well known that the design of the VSI PLL should be robust enough in order to cope with potential harmonic voltage distortions, which are expected to be prevalent in high impedance LV grids. In addition, it has been demonstrated that PLLs can introduce a low-frequency impedance that is in parallel with the open-loop impedance of the VSI [3]. Such phenomena can influence the VSI's output impedance and give rise to low-frequency power oscillations through its interaction with the grid impedance under certain conditions [3]. Finally, it has also been recently demonstrated that the grid impedance can influence the PLL dynamics through its impact on the PLL self-synchronization loop [4] and the PLL synchronization stability, which can be important during current transients [5]. The impact of the grid impedance on the PLL stability is investigated in [6].

Typically, one way to improve the PLL stability is to design the PLL with reduced bandwidth. However, this comes at the expense of making the PLL response very slow [7]. Such paradigm creates a situation where a trade-off must exist between increasing the dynamic response of the PLL and improving the stability of the VSI [8]. To effectively deal with this trade-off, there exist multiple approaches that can help in the provision of a robust control design, e.g., the H-infinity loop-shaping technique. These approaches commonly require identifying the bound of the deviation between the nominal value of the parameters used in the design and the actual values encountered in practice. On this subject, one

This work has emanated from research conducted with the financial support of Science Foundation Ireland under Grant No. SFI/16/IA/4496. The opinions, findings, and conclusions or recommendations expressed in this material are those of the authors and do not necessarily reflect the views of the Science Foundation Ireland.

The authors are with the Energy Institute and the School of Electrical and Electronic Engineering, University College Dublin, Dublin 4, Ireland.

978-1-6654-4875-8/21/$31.00 ©2021 IEEE

influential parameter is the impedance at the PV's common point of connection, Z_g, which possible variations can be characterized by exploring its magnitude under all expected operating conditions of the grid.

Multiple approaches have been proposed for characterizing the variations of Z_g in front of potential changes in the network's loads and configuration, and the local and upstream grid. In [9], the data generated from multiple operating conditions is used as an input for a clustering technique to obtain a reduced number of representative impedance patterns. The online method in [10] provides a parametric multivariate model of the network admittance. This method employs sensitivity analysis and instrumental variable method for continuous-time system identification. In [11], the authors estimate the Thevenin equivalent parameters using phasor measurement unit data. The proposed approach is tested under various IEEE test networks. Finally, the work in [12] analyses a large data set of measured access impedances at the LV level and provides stochastic models for both resistance and reactance components.

This paper proposes a stochastic representation of the grid impedance at the connection point of a PV system in an LV network. To do so, an ellipse that embraces the joint variations of the grid resistance and inductance, with a requested confidence level, is generated from the results of a series of Monte Carlo simulations. The maximum likelihood estimation (MLE) approach and confidence level analysis are employed for this purpose. This extracted ellipse expresses the codependent range of the variations of the resistance and inductance of the connection point under different operational conditions of the network. These ranges of variations can be regarded in the design of the PLL unit of the PV system. In this way, the stability of the PV system is secured under probable network operational conditions. It should be emphasized that the process of developing a robust design for the PV PLL using this extracted confidence region is addressed in our future works.

II. Methodology

In this section, Monte Carlo simulations are employed to explore different operating points of an LV network. Then, the joint probability distribution of the network's resistance and inductance at the PV's connection point is extracted and the MLE approach is employed to model the provided joint probability distribution as a 2-variate Gaussian distribution. Confidence level analysis is employed afterward to extract a region that embraces the impedance variations with a requested confidence level. Finally, a normality test is conducted.

A. Monte Carlo Analysis To Explore Impedance Variations

To capture the variations of the network impedance over a variety of network operating points, one effective approach is to obtain the probability distribution of these variations. Let Z_{Hk} denote the network impedance at the connection point Hk. Z_{Hk} consists of the resistance, R_{Hk}, and inductance, L_{Hk}, as $Z_{Hk} = R_{Hk} + j2\pi f_s L_{Hk}$, where f_s is the power system frequency. Since R_{Hk} and L_{Hk} are correlated, to obtain the probability distribution of Z_{Hk}, the joint probability distribution of R_{Hk} and L_{Hk} should be extracted.

B. Maximum Likelihood Estimation

MLE is aimed at constructing a representation of a stochastic phenomenon. Let x denote a stochastic process consisting of d stochastic variables. Assume that the probability density function (PDF) of x, i.e., f, belongs to a known parametric family of densities, i.e., $\{f(.|\theta)|\theta \in \Theta\}$, where $\theta = [\theta_1, ..., \theta_m]$ is a vector of m unknown parameters, and Θ is its corresponding parameter space. Given a set of n observations, $X = [X_1, ..., X_n]$, with X_i $(\forall i = 1, ..., n)$ a vector of size d, the objective is to find a set of parameters, $\hat{\theta}$, such that under the derived PDF, $f(x|\hat{\theta})$, the observations are most probable. This is achieved by maximizing a log-likelihood function, $\gamma(\theta|X)$, over the given observation set, as [13]:

$$\hat{\theta} = \arg\max_{\theta \in \Theta} \gamma(\theta, X) \tag{1}$$

Assuming that $\gamma(\theta|X)$ is differentiable in θ, a necessary condition for $\hat{\theta}$ to maximize $\gamma(\theta|X)$ in (1) is that the partial derivatives of $\gamma(\theta|X)$ with respect to all the parameters at $\hat{\theta}$ be equal to zero, as [13]:

$$\big(\partial\gamma/\partial\theta_j\big)|_{\hat{\theta}} = 0 \quad \forall j = 1, .., m \tag{2}$$

Solving the set of equations in (2) yields the optimum set of parameters for the assumed distribution.

C. Maximum Likelihood for Impedance Characterization

Here, the Gaussian distribution is employed to describe the joint probability distribution of R_{Hk} and L_{Hk}, as (3), where g represents the PDF of R_{Hi} and L_{Hi}. g contains the mean vector, M_{Hi}, and the covariance matrix, Σ_{Hi}. The suitability of the 2-variate Gaussian distribution for this problem is examined using the kurtosis test, in Subsection II-E.

$$g\Big([R_{Hk}, L_{Hk}]|\{M_{Hk}, \Sigma_{Hk}\}\Big) = \big(1/(2\pi|\Sigma_{Hk}|)^{0.5}\big)\times \exp\Big(([R_{Hk}, L_{Hk}] - M_{Hk})\Sigma_{Hk}^{-1}([R_{Hk}, L_{Hk}] - M_{Hk})^T\Big) \tag{3}$$

Considering (3), for each connection point, Hk, the corresponding parameters, i.e., M_{Hi}, and Σ_{Hi}, should be estimated. To this end, given the provided samples of R_{Hk} and L_{Hk} by Monte Carlo simulations, the log-likelihood function is constructed as in (1) and the set of equations in (2) is solved. Consequently, the optimal estimation for M_{Hi}, and Σ_{Hi}, denoted by $\hat{M_{Hi}}$, and $\hat{\Sigma_{Hi}}$, are achieved.

D. Confidence Level To Capture Impedance Variations

Different phenomena can cause the network impedance seen at the PV connection point to change, i.e., change of the value, power factor, and type of the demand of different network buses, change of the topology of the LV feeder, change of the impedance of the upstream network, change of the voltage of

the head of the feeder, and integration of distributed energy resources at other network nodes. The impact of some of these phenomena on the network impedance and the performance of the proposed approach to capture the impedance variations under these scenarios are investigated in the following section.

The main purpose of modeling the probability distribution of the samples via a Gaussian distribution is to capture the range of the variations of R_{Hk} and L_{Hk} to design a robust PLL. The confidence level analysis is a prominent method for this purpose. Given $\hat{M_{Hi}}$, and $\hat{\Sigma_{Hi}}$, and considering a desirable confidence level, α, the confidence level analysis proposes an ellipse that encounters the data samples with a probability of α as [14]:

$$E = \{y \in \mathbb{R}^2 | (y - M_{HK})\Sigma_{HK}^{-1}(y - M_{HK})^T = r^2\} \quad (4)$$

where E determines the perimeter of this ellipse, and r is the Mahalanobis distance, given as:

$$r = \sqrt{-2\log(1-\alpha)} \quad (5)$$

In our study, a confidence level of 95% is considered to include the majority of L_{Hk} and R_{Hk} variations. The 95% confidence ellipse achieved by (4) is denoted by 95-CE.

E. Kurtosis for Normality Test

There are several measures to test the normality of a data set, i.e., whether the Gaussian distribution is a suitable fit for describing the distribution of the data samples. Here, the main purpose of employing the 2-variate Gaussian distribution is to extract the 95% confidence regions. Therefore, the most important feature is that the fitted Gaussian model has effectively embraced the data samples that are away from the mean. A suitable test for this purpose is to evaluate the kurtosis of the data samples and compare it to the kurtosis of an ideal Gaussian distribution. Kurtosis is the fourth standardized central moment of a distribution. Considering the data samples $X = [X_1, ..., X_n]$ in Subsection II-C, kurtosis is defined as [15]:

$$\kappa = \big(\sum_{i=1}^{n} |(X_i - M_{HK})\Sigma_{HK}^{-1}(X_i - M_{HK})^T|^2\big)/n \quad (6)$$

where κ stands for the kurtosis of X, and $|.|$ denotes the euclidean norm operator.

Given that kurtosis is proportional to the fourth central moment, it naturally gives higher importance to the data samples that are away from the mean of the distribution. Therefore, kurtosis highlights the departure from normality on the tails of the distribution which is, as stated, more favorable for the proposed modeling approach.

Fig. 1 summarizes the algorithm applied in this paper for the grid impedance characterization.

III. Results

A. Test System

The Cigre LV distribution benchmark for residential European feeders is considered as the test system [16]. This system serves 6 loads with an overall rated power of 404 kVA. This network is modified by integrating three single-phase loads at buses 11, 15, and 18, with a rated power of 15, 10, and 8 kVA, respectively. These loads represent the household consumers that intend to be equipped with a PV system. Therefore, the impedance of the network is analyzed from these connection points, i.e, $H1$, $H2$, and $H3$, respectively. Fig. 2 depicts a schematic diagram of this feeder.

B. Monte Carlo Analysis

Analyzing the Irish standard load profiles in 2019 [17], provided by ESB Networks (an Irish electricity supply company), reveals that the ratio of the mean of annual consumption to the rated power, denoted by μ, is 0.4 for residential consumers in Ireland. In addition, the coefficient of variation, CV, is equal to 0.4, where CV is defined as the ratio of mean to standard deviation. It is also assumed that a correlation of 0.6 exists between the consumption values corresponding to each pair of network loads. Let ρ denote this correlation. The power factor of each load is a random number between 0.9 lag to 1. Loads are assumed to behave as purely constant active and reactive power (Constant PQ). Monte Carlo simulations generate 10,000 pairs of active and reactive powers for each network load. EPRI's OpenDSS (a distribution system simulator) is employed to run the power flow equations. Consequently, 10,000 operating points are provided for this test network. Afterward, at each operating point, the network's impedance at each of the considered connection points is evaluated by injecting a small-signal current into the connection point, ΔI_{Hi}, followed by calculating the corresponding node voltage variation, ΔV_{Hi}, and then finding the ratio of ΔV_{Hi} to ΔI_{Hi}, as $Z_{Hi} = \Delta V_{Hi}/I_{Hi}$ ($\forall i = 1, 2, 3$). Having Z_{Hi}, R_{Hk} and L_{Hk} can easily be evaluated. Therefore, three data sets are provided for the MLE analysis.

C. Results of The MLE Analysis

The MLE analysis is employed on the provided data sets to extract the Gaussian distribution of R_{Hk} and L_{Hk}. Figs. 3, 4, and 5 show the actual joint probability distribution of R_{Hk} and L_{Hk}, together with the fitted Gaussian distribution by MLE. Table I presents the corresponding κ of each data set. The kurtosis of an ideal 2-variate Gaussian distribution equals 8 [15]. As seen, for all the connection points, the value of the evaluated κ is close to the kurtosis of an ideal Gaussian distribution, which verifies that the Gaussian distribution is a suitable fit for modeling the distribution of these data sets.

D. Results of The Confidence Level Analysis

Following the extraction of the Gaussian distributions, the confidence level analysis is employed to construct the 95-CEs. These ellipses represent the range of the variation of R_{Hk} and L_{Hk}, with a confidence level of 95%. To examine the accuracy of the proposed approach, the portion of the data samples placed inside the extracted 95-CEs are evaluated. Table I presents the results. As seen, for all the connection points, this portion is very close to the expected 95%, which

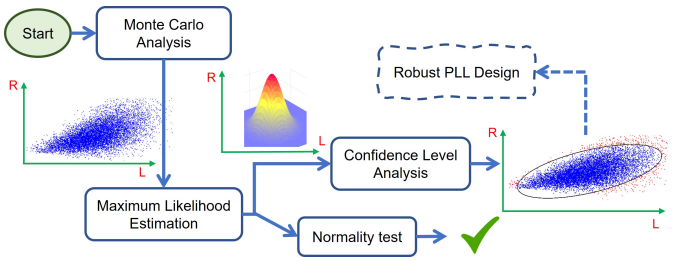

Fig. 1. The block diagram of the proposed approaches.

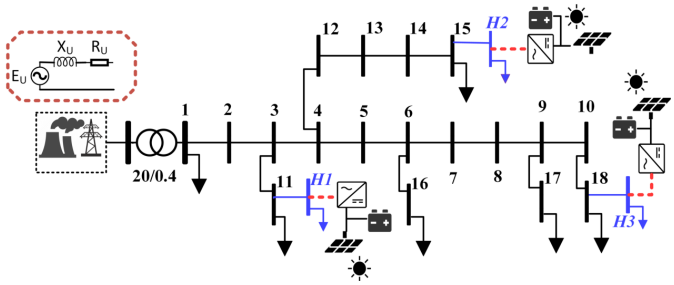

Fig. 2. The schematic diagram of the CIGRE LV distribution feeder.

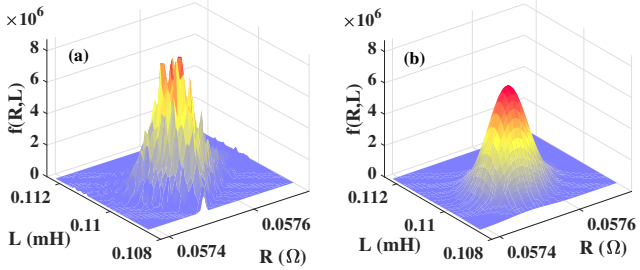

Fig. 3. The joint probability distribution of R_{H1} and L_{H1}: a) simulation results, b) the fitted Gaussian distribution.

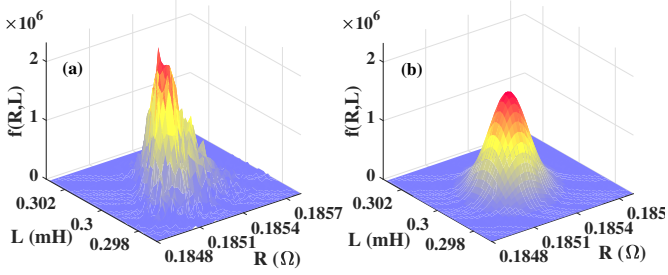

Fig. 4. The joint probability distribution of R_{H2} and L_{H2}: a) simulation results, b) the fitted Gaussian distribution.

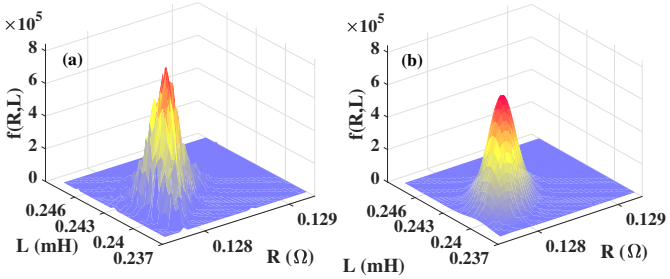

Fig. 5. The joint probability distribution of R_{H3} and L_{H3}: a) simulation results, b) the fitted Gaussian distribution.

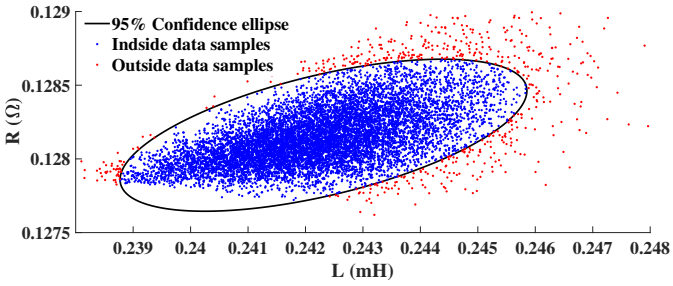

Fig. 6. The 95-CE corresponding to $H3$, together with the data samples.

emphasizes that the extracted 95-CEs effectively represent the variations of the network impedance. As an example, Fig. 6 shows the 95-CE corresponding to $H3$, together with the Monte Carlo data samples. This figure demonstrates how the extracted 95-CE encircles around 95% of the data samples.

To study how the 95-CEs are influenced by the variation of network parameters, different study cases are constructed by altering one of the parameters at each step, while keeping the others as the main study case. On this subject, at first, besides $\rho = 0.4$, two other values are considered for ρ, i.e., 0.4, and 0.8. Then, besides $\mu = 0.4$, and $CV = 0.4$, two other values are considered for CV, and μ, i.e., $CV = 0.2$, $CV = 0.6$, $\mu = 0.3$, and $\mu = 0.5$. Afterward, the impedance of the upstream network, Z_u, is altered by $\pm 10\%$, i.e., $Z_u = 0.9Z0_u$, and $Z_u = 1.1Z0_u$, where $Z0_u$ represents the original value of Z_u. Finally, the types of the network loads are changed to constant impedance (Constant Z), and constant current (Constant I).

Figs. 7, 8, and 9 show the 95-CEs corresponding to the connection points $H1$, $H2$, and $H3$, respectively, for different values of ρ, CV, and μ. As seen, a change in ρ does not influence the 95-CEs noticeably, whereas an increase in CV makes the CEs taller along the major axis, symmetrically. The influence of a change in μ depends on the connection point: for $H1$ and $H3$, the 95-CEs expand towards the major axis, but for $H2$, the 95-CEs expand along both of the axes. The main reason for such patterns can be found by considering that with an increase in CV, the network loads vary in a wider range, mostly symmetrically around μ, therefore, the 95-CEs are expected to expand symmetrically. An increase in μ, however, means the network is experiencing a higher level of loading. In this regard, the feeder that connects $H2$

TABLE I
THE RESULTS OF THE NORMALITY TEST

Connection point	*H1*	*H2*	*H3*
Kurtosis of the data samples	9.63	9.63	9.79
Portion of data samples inside the 95-CEs (%)	94.6	94.4	94.5

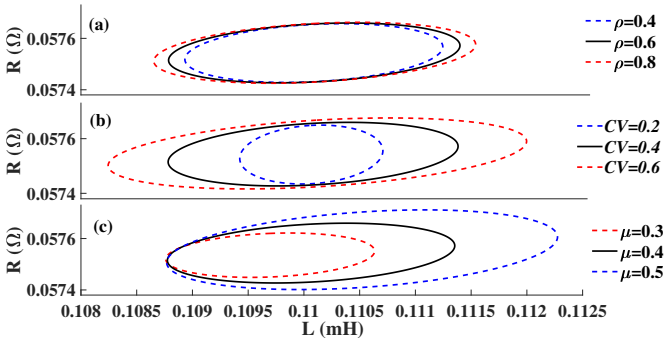

Fig. 7. The CEs corresponding to the $H1$ connection point with different values for the loads' stochastic parameters: a) ρ, b) CV, c) mu.

to node 4 has quite different characteristics than the one that connects $H1$ and $H3$ to the head of the feeder: the impedance of the former is around 3.7 times larger (ohms/km), and the resistance to reactance ratio is around 1.5 times higher (2.5 to 1.7). Therefore, an increase in μ has different influences on the 95-CEs of $H2$ compared to those of $H1$, and $H3$.

Fig. 10 presents the impact of Z_u on 95-CEs, for different connection points. As seen, a change in Z_u just shifts the 95-CEs along the direction of the decrease or increase in Z_u: to a moderate extent for $H1$, which is closer to the head of the feeder, and to a lesser extent for $H2$, and $H3$. Therefore, it can be concluded that for practical European feeders that are generally longer than this benchmark feeder, modeling the variations of Z_u is not of high importance, unless the connection point is near to the head of the feeder.

Fig. 10 depicts the 95-CEs when different types of loads are examined. As seen, the load type has a significant impact on the 95-CEs, for all the connection points. On this subject, not only the 95-CEs have been shifted in Fig. 11, but also the area of the 95-CEs has changed to a great extent. This emphasizes the importance of having a precise model of the load types when the stability of the PV's PLL is the subject of a study in LV distribution networks.

IV. CONCLUSION

The MLE approach, together with the confidence level analysis, was employed to present a stochastic representation of the network impedance seen at the point of the connection of a PV system to an LV distribution network. In this regard, an ellipse was constructed that embraces the variations of the resistance and inductance of the connection point together, with a confidence level of 95%. Results show that the shape and characteristics of these ellipses are highly dependant on the location of the connection point. It was also concluded that whilst the stochastic properties of the network loads can

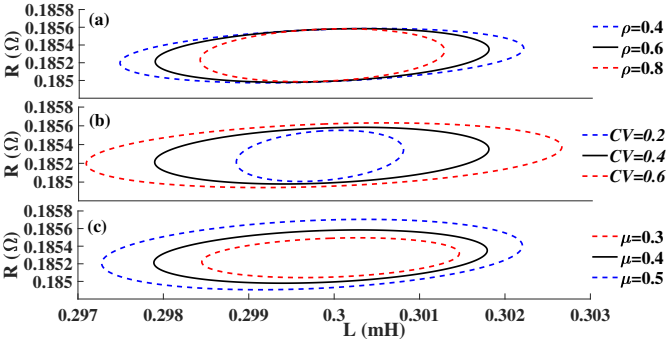

Fig. 8. The CEs corresponding to the $H2$ connection point with different values for the loads' stochastic parameters: a) ρ, b) CV, c) mu.

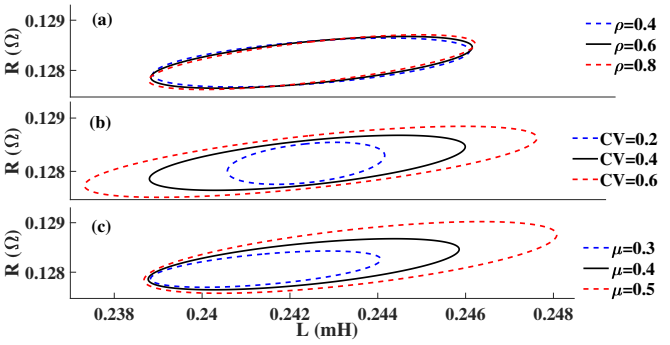

Fig. 9. The CEs corresponding to the $H3$ connection point with different values for the loads' stochastic parameters: a) ρ, b) CV, c) mu.

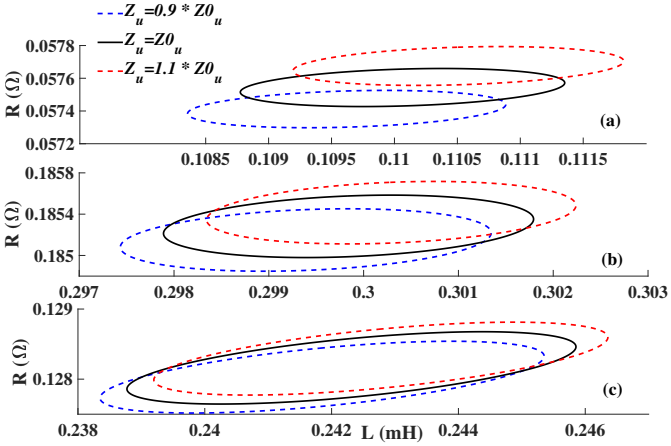

Fig. 10. The impact of Z_u on CEs at connection points: a) $H1$, b) $H2$, and c) $H3$.

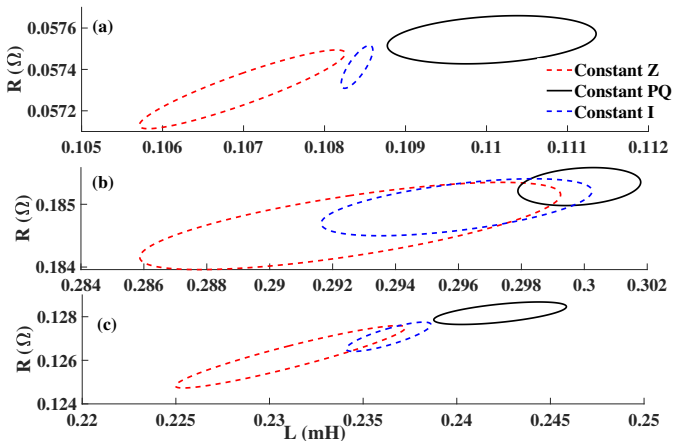

Fig. 11. The CEs with different load types, at different connection points: a) $H1$, b) $H2$, and c) $H3$.

affect the shape of these ellipses, but the most important feature is the type of the loads. Therefore, to accurately model the variations of the network impedance, it is of prominent importance to have a precise model of the network loads, which will be considered in our future studies. The provided stochastic representation of the network impedance in this work determines the bound of the variations of this impedance. This bound can subsequently be considered when a robust control design technique is meant to be applied to set the control parameters of the PV's PLL, which is the subject of our future work.

In this paper, the proposed approach was implemented on a relatively small LV feeder. It would be interesting to test this approach on more realistic large-scale LV feeders to investigate its performance. In addition, instead of using only one Gaussian distribution to model the distribution of the network impedance, a mixture of Gaussian distributions could have been applied which may result in more accurate results. Another thing that could have been regarded in this analysis is to consider the change of the topology of the LV feeder and investigate if this approach can still effectively model the variations of the network impedance under different topologies.

REFERENCES

[1] P. Rodriguez, J. Pou, J. Bergas, J. I. Candela, R. P. Burgos, and D. Boroyevich, "Decoupled double synchronous reference frame pll for power converters control," *IEEE T. Power Electron.*, vol. 22, no. 2, pp. 584–592, 2007.

[2] M. M. de Carvalho, R. L. P. Medeiros, I. V. Bessa, F. A. C. Junior, K. E. Lucas, and D. A. Vaca, "Comparison of the pll control techniques applied in photovoltaic system," in *2019 IEEE 15th Brazilian Power Electronics Conference and 5th IEEE Southern Power Electronics Conference (COBEP/SPEC)*, 2019, pp. 1–6.

[3] B. Wen, D. Boroyevich, P. Mattavelli, Z. Shen, and R. Burgos, "Influence of phase-locked loop on input admittance of three-phase voltage-source converters," in *2013 Twenty-Eighth Annual IEEE Applied Power Electronics Conference and Exposition (APEC)*, 2013, pp. 897–904.

[4] D. Dong, B. Wen, D. Boroyevich, P. Mattavelli, and Y. Xue, "Analysis of phase-locked loop low-frequency stability in three-phase grid-connected power converters considering impedance interactions," *IEEE T. Ind Electron*, vol. 62, no. 1, pp. 310–321, 2015.

[5] J. Chen, M. Liu, T. O'Donnell, and F. Milano, "Impact of current transients on the synchronization stability assessment of grid-feeding converters," *IEEE T. Power Syst.*, vol. 35, no. 5, pp. 4131–4134, 2020.

[6] M. Berg, A. Aapro, R. Luhtala, and T. Messo, "Small-signal analysis of photovoltaic inverter with impedance-compensated phase-locked loop in weak grid," *IEEE Transactions on Energy Conversion*, vol. 35, no. 1, pp. 347–355, 2020.

[7] M. Cespedes and J. Sun, "Adaptive control of grid-connected inverters based on online grid impedance measurements," *IEEE Transactions on Sustainable Energy*, vol. 5, no. 2, pp. 516–523, 2014.

[8] M. Davari and Y. A. I. Mohamed, "Robust vector control of a very weak-grid-connected voltage-source converter considering the phase-locked loop dynamics," *IEEE T. Power Electron.*, vol. 32, pp. 977–994, 2017.

[9] C. Li, M. Molinas, O. B. Fosso, N. Qin, and L. Zhu, "A data-driven approach to grid impedance identification for impedance-based stability analysis under different frequency ranges," in *2019 IEEE Milan PowerTech*, 2019, pp. 1–6.

[10] M. A. Azzouz and E. F. El-Saadany, "Multivariable grid admittance identification for impedance stabilization of active distribution networks," *IEEE T. Smart Grid*, vol. 8, no. 3, pp. 1116–1128, 2017.

[11] H. Su and T. Liu, "Robust thevenin equivalent parameter estimation for voltage stability assessment," *IEEE T. Power Syst.*, vol. 33, no. 4, pp. 4637–4639, 2018.

[12] B. Uzum, A. Onen, H. M. Hasanien, and S. M. Muyeen, "Rooftop solar pv penetration impacts on distribution network and further growth factors—a comprehensive review," *Electronics*, vol. 10, no. 1, 2021.

[13] R. B. Miller, *Maximum Likelihood Estimation and Inference*. John Wiley & Sons, Ltd, 2011, ch. 2, pp. 18–35.

[14] W. Hardle and L. Simar, *Applied Multivariate Statistical Analysis*, 4th ed. Springer-Verlag Berlin Heidelberg, 2015.

[15] M. Cain, Z. Zhang, and K. Yuan, "Univariate and multivariate skewness and kurtosis for measuring nonnormality: Prevalence, influence and estimation," *Behavior R. Methods*, vol. 49, no. 5, p. 1716–1735, 2017.

[16] K. Strunz, E. Abbasi, R. Fletcher, N. Hatziargyriou, R. Iravani, and G. Joos, "Benchmark systems for network integration of renewable and distributed energy resources," CIGRE, Tech. Rep. TB 575, 2014.

[17] "ESB Standard Load Profiles," online, accessed 17/12/2020, https://rmdservice.com/standard-load-profiles/.